NASA/TM—2001-210807

Development of Tough, Strong, and Pest-Resistant $MoSi_2$-βSi_3N_4 Composites for High-Temperature Structural Applications

M.G. Hebsur and S.R. Choi
Ohio Aerospace Institute, Brook Park, Ohio

J.D. Whittenberger, J.A. Salem, and R.D. Noebe
Glenn Research Center, Cleveland, Ohio

Prepared for the
International Symposium on Structural Intermetallics
cosponsored by The Minerals, Metals, and Materials Society and the
American Institute of Mining, Metallurgical, and Petroleum Engineers
Jackson Hole, Wyoming, September 23–25, 2001

National Aeronautics and
Space Administration

Glenn Research Center

May 2001

Acknowledgments

Financial support for this work came from the HOTPC program at NASA Glenn Research Center, Cleveland, Ohio.

This report contains preliminary findings, subject to revision as analysis proceeds.

Available from

NASA Center for Aerospace Information
7121 Standard Drive
Hanover, MD 21076

National Technical Information Service
5285 Port Royal Road
Springfield, VA 22100

Available electronically at http://gltrs.grc.nasa.gov/GLTRS

DEVELOPMENT OF TOUGH, STRONG AND PEST-RESISTANT $MoSi_2$-βSi_3N_4 COMPOSITES FOR HIGH-TEMPERATURE STRUCTURAL APPLICATIONS

M.G. Hebsur and S.R. Choi
Ohio Aerospace Institute
Brook Park, Ohio 44142

J.D. Whittenberger, J.A. Salem, and R.D. Noebe
National Aeronautics and Space Administration
Glenn Research Center
Cleveland, Ohio 44135

Abstract

A new $MoSi_2$-base composite was developed that contains *in-situ* reinforcement of whisker-type β-Si_3N_4 grains in a $MoSi_2$ matrix. The advantages of this *in-situ* reinforced $MoSi_2$-Si_3N_4 are lower density, higher fracture toughness and better strength than typical $MoSi_2$ alloys, combined with excellent environmental and pest resistance. The average fracture toughness of the *in-situ* reinforced material determined by one technique was 12.2 MPa$\sqrt{m}$ compared to 4.9 to 5.5 MPa$\sqrt{m}$ for similar materials with the exception that the β-Si_3N_4 had a blocky morphology as opposed to the whisker-like morphology typical of the *in-situ* toughened material. This $MoSi_2$-βSi_3N_4 was also resistant to pesting at intermediate temperatures (400 to 600 °C) even when precracked or under applied load; conditions that would quickly reduce typical $MoSi_2$ alloys to oxidized powder.

1. Introduction

Due to its excellent high-temperature oxidation resistance, low density, and high thermal conductivity, $MoSi_2$ is one of a few attractive intermetallic systems still being considered for structural applications. But like many ordered intermetallics, it is brittle at low temperatures, weak at high temperatures, and suffers from pesting or accelerated oxidation at intermediate temperatures [1]. However, previous work has shown that the addition of 30 to 50 vol % of Si_3N_4 to $MoSi_2$ eliminated pesting by forming a protective silicon oxynitride (Si_2ON_2) scale instead of the usual MoO_3 [2]. The Si_3N_4 additions also doubled the room-temperature fracture toughness, decreased the 1200 °C compressive creep rates by nearly five orders of magnitude, and lowered the coefficient of thermal expansion (CTE) of $MoSi_2$ [3]. Further improvements in toughness and elevated temperature strength were achieved by reinforcing the $MoSi_2$-Si_3N_4 matrix with about 30 vol % of SiC continuous fibers [4]. The SiC fiber reinforcement improved the room-temperature fracture toughness by an additional factor of seven and charpy impact energy by about five times compared to the $MoSi_2$-Si_3N_4 matrix. This hybrid composite maintained its excellent strength and toughness improvements up to 1400 °C. Good strength and toughness were also obtained by reinforcing the $MoSi_2$-Si_3N_4 with fine diameter Hi-Nicalon fibers. This hybrid composite was successfully tested in Pratt and Whitney's demonstrator engine, XTC/66/b, in a blade outer air seal simulation [5,6].

Tape casting was adopted as the preferred processing route for $MoSi_2$-Si_3N_4 fiber composites in the previous studies [4–6] because of the improved fiber spacing, ability to use fine diameter fibers, and relatively low processing costs. However, manufacturing of state-of-the-art fiber-reinforced composites is still quite expensive due to the high cost of fibers and fiber coatings. Slurry infiltration of SiC fiber 3D preforms by $MoSi_2$-Si_3N_4 followed by melt infiltration with molten silicon might be one alternative to reduce costs. But the excess silicon in the composite might adversely influence the long-term creep properties.

Consequently, the objective of this investigation is to produce a new $MoSi_2$-base alloy that exhibits excellent pest resistance at intermediate temperatures (500 °C), excellent oxidation resistance at elevated temperatures, and more importantly, has very high fracture toughness and reliability so that fiber reinforcement is no longer necessary. This has been achieved by reinforcing a $MoSi_2$-base alloy with a high volume fraction of randomly oriented, *in-situ* grown, long whisker-type grains of β-Si_3N_4. This engineered microstructure is produced through proper thermomechanical treatment and the use of sintering additives, which promote the growth of long whiskers of β-Si_3N_4 in a fully dense $MoSi_2$ matrix. The combination of properties

achieved by this new alloy would make it a viable alternative to conventional materials for such aerospace applications as a blade outer air seal or as exhaust nozzle and combustor components. Other suitable applications include automotive glow plugs and use as a protective coating for Mo-base alloys [7].

2. Experimental

2.1 Processing of In-Situ Toughened $MoSi_2$-Si_3N_4

A series of processing runs, summarized in table I, were made in order to determine the minimum requirements necessary to produce a fully dense material with the desired *in-situ* toughened microstructure composed of whisker-like Si_3N_4 grains. The starting material for all processing runs consisted of a mixture of 50 percent by volume of -325 mesh $MoSi_2$ powder of at least 98.5 percent purity purchased from Aesar Inc., and 1 to 2 μm Si_3N_4 powder obtained from HC Stark, Inc. Sintering aids were added to three of the processing runs to help promote growth of the Si_3N_4 into whisker-shaped grains. These additives consisted of about 1 wt.% of nano sized Y_2O_3 and 4 wt.% of nano sized Al_2O_3, both obtained from Nanotek, Inc.

The powder mixtures were first blended in batches in a SiC jar mill consisting of 700 grams of charge material and 1500 grams of SiC grinding media (6-mm-diameter balls) for 24 hr. The blended mixture was further milled for 8 hr in a Union Process Model Research 1-S attritor using 6-mm-diameter WC grinding media and an impeller rotation speed of 450 rpm. The ball to powder ratio was 20:1. To achieve efficient grinding, the outer jacket of the attritor was cooled with continuously flowing liquid nitrogen. After 8 hr of milling, the powder was separated anaerobically from the grinding media in a glovebox containing an argon atmosphere. Particle size analysis of the $MoSi_2$-50 vol % Si_3N_4 mixture revealed that the average mean particle size of the mixture was 1.25 ± 0.71 μm at 99 percent confidence.

Several batches $MoSi_2$-Si_3N_4 with sintering additives were also prepared in a Union Process Model 01-HD attritor. In this case, 6-mm diameter 440 stainless steel balls were used instead of the WC grinding media. Each batch consisted of 400 g of powder mixture ground for about 8 hr with an impeller speed of 500 rpm. Unfortunately, some powder loss occurred due to a faulty seal but in total about 1800 g of powder was produced by this technique and consolidated under the conditions identified for alloy MS-80.

The $MoSi_2$-Si_3N_4 powder mixtures, with and without sintering aids, were consolidated under the various conditions listed in table I. For example, alloy MS-60 was hot pressed into 5 cm long × 5 cm wide × 0.3 cm thick plates by vacuum hot pressing at 1400 °C at 120 MPa for 2 hr, which resulted in about an 85 percent dense compact. The hot pressed plate was then sandwiched between SiC backing plates and then the entire structure was enclosed in a 0.76-mm-thick Ta can, which was evacuated and sealed using an electron beam welder. Further consolidation of the hot pressed plate was achieved by hot isostatic pressing (HIP'ing) at 1900 °C/300 MPa for 2 hr. The resulting material was fully dense and contained the desired β-Si_3N_4 whisker-type morphology.

Hot pressing at higher temperatures (1600 and 1800 °C) generally resulted in severe flashing and reaction with the graphite dyes. However, hot pressing at 1800 °C did result in a fully dense and intact specimen, which could then be further processed by HIP'ing without the need for a Ta can (alloy MS-70). Additional processing of the dense compact at the higher HIP temperature was still necessary in order to promote the *in-situ* growth of the whisker-like β-Si_3N_4 grains. During processing of alloy MS-80, it was found that a thin

Table I.—Processing Conditions for the various alloys investigated

Alloy designation	Alloy composition, wt.%	Consolidation conditions	Microstructure
MS-60	$MoSi_2$-35Si_3N_4-4Al_2O_3-1Y_2O_3	Hot Press: 1400 °C/120 MPa/2-hrs HIP (Ta can): 1900 °C/300 MPa/2-hrs	Fully dense β-Si_3N_4 with long whisker-type morphology
MS-70	$MoSi_2$-35Si_3N_4-4Al_2O_3-1Y_2O_3	Hot Press: 1800 °C/70 MPa/3-hrs HIP (no can necessary): 1900 °C/300 MPa/2-hrs	Fully dense β-Si_3N_4 with long whisker-type morphology
MS -80	$MoSi_2$-35Si_3N_4-4Al_2O_3-1Y_2O_3 (Processed in 01-HD attritor with significant powder loss)	Hot Press: 1600 °C/56 MPa/2-hrs + 1700 °C/56 MPa/2-hrs HIP (graphoil wrap): 1900 °C/280 MPa/2-hrs	Not fully dense β-Si_3N_4 with blocky morphology
MS-50	$MoSi_2$-35Si_3N_4	Hot Press: 1400 °C/120 MPa/2-hrs HIP (Ta can): 1500 °C/300 MPa/2-hrs	Fully dense α-Si_3N_4 with blocky morphology
MS-40	$MoSi_2$-35Si_3N_4	Hot Press: 1200 °C/200 MPa/2-hrs HIP (Ta can): 1200 °C/280 MPa/2-hrs.	Not fully dense Fine grained $MoSi_2$ and blocky α-Si_3N_4

layer of BN was effective in preventing the flashing. However during HIP'ing at higher temperatures the BN diffused into the alloy and possibly prevented the β-Si_3N_4 grain growth. It is also possible that much of the fine sintering aids could have been lost due to the seal leak when processing the powder used for this alloy in the 01-HD attritor. Furthermore, hot pressing at temperatures as high as 1700 °C did not produce a fully dense compact. Even so these panels were HIPed without enclosing in a tantalum can but failed to fully densify because the porosity must have been interconnected. Processing conditions for other materials studied or compared in this investigation are summarized in table I.

2.2 Testing Procedures

From the consolidated material, specimens for determining physical, mechanical, and environmental properties were machined using electro-discharge machining (EDM) and grinding techniques. Basic room-temperature physical properties such as density, dynamic elastic modulus, coefficient of thermal expansion, and Vickers microhardness were evaluated for alloy MS-70. The density of three flexural specimens was determined using the volume-mass method. The dynamic elastic modulus was determined at various temperatures by the impulse excitation method (ASTM C 1259) using flexural specimens. Vickers microhardness was estimated at an indentation load of 98 N by averaging five measurements on each of two specimens according to ASTM C 1327.

Compression strengths were measured using 4-mm dia × 8-mm long cylindrical specimens. Compression tests were conducted between room temperature and 1400 °C in air using a screw-driven Instron machine. Compression specimens were also used to investigate pesting at 500 °C under compressive loading.

Room-temperature fracture toughness was determined using four different methods: indentation fracture (IF), single edged v-notched beam (SEVNB) [8], single edged precracked beam (SEPB; ASTM C 1421), and chevron-notched beam (CNB; ASTM C 1421). In the IF method, a total of five indents were used at each of two indentation loads of 98 and 196 N. Three specimens were used with both the SEPB and SEVNB methods with crack size-to-specimen ratios ranging from 0.25-0.6. The chevron-notched beam specimens measured 3- × 6-mm in cross-section by 50-mm long. Testing was conducted in an Instron test machine fitted with a four-point bend fixture. A valid K_{Ic} was determined from load-displacement data and specimen initial dimensions using a slice finite element model [9].

Flexural strength of $MoSi_2$-βSi_3N_4 (MS-70) was measured using ASTM standard modulus of rupture (MOR) bar specimens (3-mm thick × 4-mm wide × 50-mm long) at various temperatures between room temperature and 1400 °C in air. MOR bars 3-mm thick and 4-mm wide by 20-mm long were machined to measure the bend strength and Weibull modulus of MS-70 and MS-80 at room temperature.

3. Results

3.1 Microstructure

Figure 1(a) shows a SEM back scattered image of a fully dense $MoSi_2$-βSi_3N_4 composite (MS-70). During processing, the original

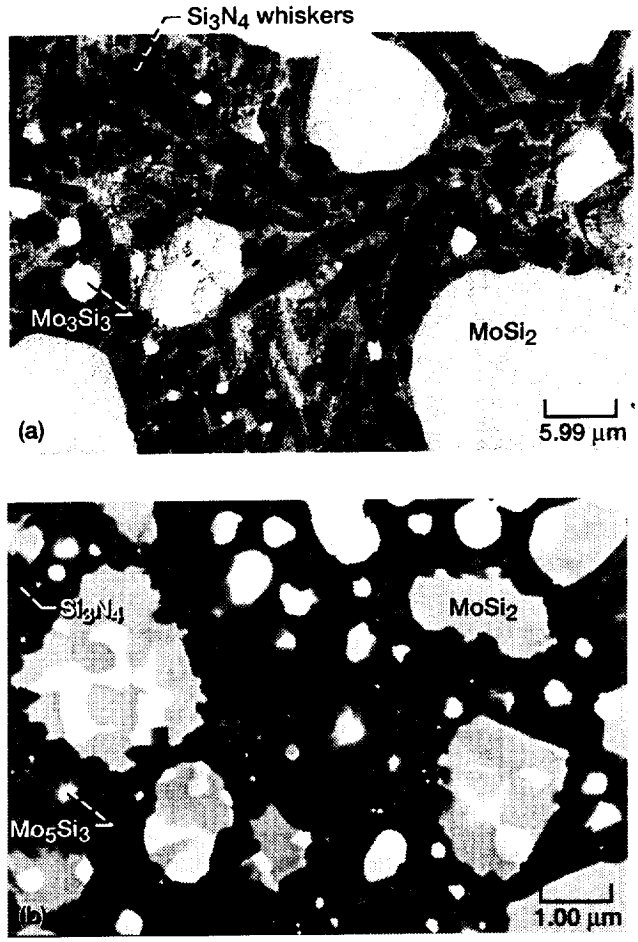

Figure 1.—(a) SEM back scattered image of $MoSi_2$-βSi_3N_4 (MS-70) showing randomly oriented *in-situ* grown long whiskers of β-Si_3N_4 and large $MoSi_2$ particle size. (b) SEM back scattered image of $MoSi_2$-βSi_3N_4 (MS-80) where the Si_3N_4 has a blocky particulate structure and not a whisker-like morphology.

α-Si_3N_4 powder particles are transformed into randomly oriented whiskers of β-Si_3N_4. These long whiskers are well dispersed throughout the material and appear to be quite stable, with very little or no reaction with the $MoSi_2$, even at 1900 °C. In some isolated areas, the Mo_5Si_3 phase was detected. This is due to the lack of precise compositional control in the commercially available $MoSi_2$ powders, since $MoSi_2$ is a line compound. In contrast to figure 1(a), 1(b) shows a back-scattered image of $MoSi_2$-βSi_3N_4 (MS-80) with the β-Si_3N_4 exhibiting a blocky aggregate-type morphology. There are a number of possible explanations for why the β-Si_3N_4 in this alloy did not evolve into the whisker-like morphology shown in figure 1(a). These have been discussed previously in section 2.1.

3.2 Physical Properties

So that data would be available for comparison and design purposes, physical properties were determined for the *in-situ* toughened $MoSi_2$-βSi_3N_4 (alloy MS-70). Density was measured at 4.57 ± 0.01 g/cm and Vickers microhardness was 10.7 ± 0.6 GPa. Figure 2 shows the

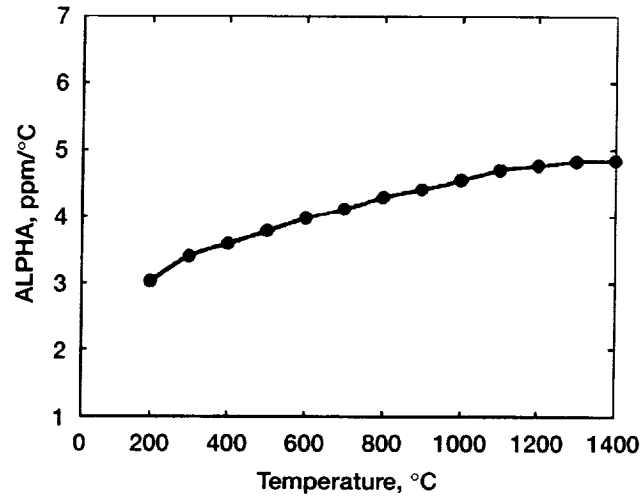

Figure 2.—The coefficient of linear expansion verses temperature for $MoSi_2$-βSi_3N_4 (MS-70) material.

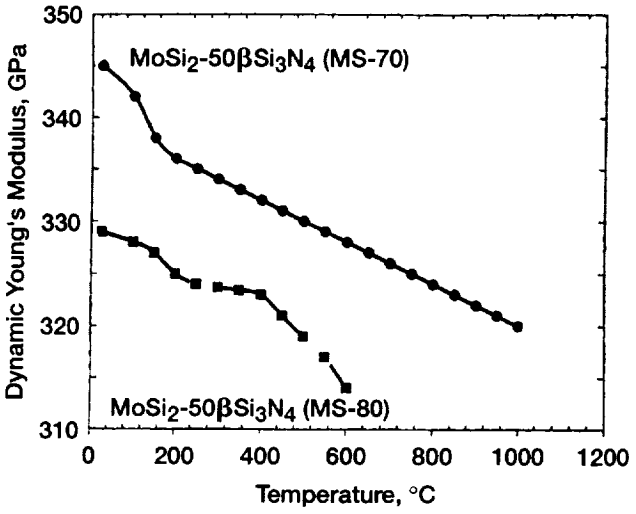

Figure 3.—Dynamic Young's Modulus verse temperature for $MoSi_2$-βSi_3N_4 materials MS-70 and MS-80.

coefficient of thermal expansion as a function of temperature for MS-70. From this data the average coefficient for expansion of this composite material is about 4.0 ppm/°C

Dynamic Young's Modulus Figure 3 shows the dynamic Young's Modulus for two batches of $MoSi_2$-βSi_3N_4 (MS-70 and MS-80) as a function of temperature. Young's Modulus for MS-70 decreases with increasing temperature but only by about 10 percent over a 1000 °C range. As expected, the denser alloy (MS-70) exhibits a higher modulus at all temperatures compared to MS-80, which contained residual porosity after processing.

Electrical Conductivity Electrical conductivity is a very important property in determining whether a material can be suitably machined by electro-discharge-machining (EDM); a widely accepted, low cost, noncontact machining technique. Room temperature electrical conductivity of various $MoSi_2$-base materials and a Si_3N_4 ceramic were

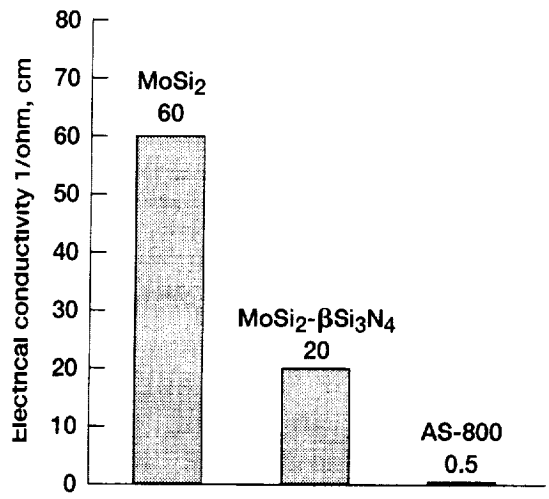

Figure 4.—Room-temperature electrical conductivity of $MoSi_2$-Si_3N_4 (MS-70) and its constituent components.

measured on rectangular bars (6-mm wide × 3-mm thick × 50-mm long). Figure 4 clearly shows more than an order of magnitude higher conductivity for the $MoSi_2$-βSi_3N_4 (MS-70) composite compared to AS-800, which is a structural Si_3N_4 ceramic. Both the $MoSi_2$ and $MoSi_2$-βSi_3N_4 have proven machineable by EDM, which was used in the fabrication of many of the test samples used in this study. In contrast, AS-800 cannot be EDM'ed, reducing the number of viable machining processes that can be used in the fabrication of components.

3.3 Mechanical Properties of Various $MoSi_2$-Si_3N_4 Materials

Compression Strength The compression yield strengths of (MS-80) measured between room temperature and 1400 °C are shown in figure 5. For comparison the compression strengths of $MoSi_2$-αSi_3N_4 (MS-50) are also included. Both materials contain 50 vol % of Si_3N_4 but figure 5 clearly indicates that $MoSi_2$-βSi_3N_4 has higher strength than $MoSi_2$-αSi_3N_4 at all temperatures. Furthermore, the MS-80 material has less than optimum microstructure and it would be anticipated that the *in-situ* toughened MS-70 or MS-60 material would exhibit even better strength, especially at high temperatures.

Fracture Toughness A summary of the fracture toughness values for in-situ toughened $MoSi_2$-βSi_3N_4 (MS-70) determined by four different test methods is presented in table II.

The SEVNB method yielded the lowest value of fracture toughness (7.4 MPa$\sqrt{m}$) and the CNB method resulted in the highest value (12.2 MPa$\sqrt{m}$). A few CNB specimens machined from MS-60 exhibited even higher fracture toughness values of 14.5 MPa $\sqrt{m}$. This is consistent with observations, that the SEVNB method tends to provide a lower value of fracture toughness particularly for aluminas [8], presumably due to rising R-curve behavior. When a material exhibits a rising R-curve, fracture toughness depends on the crack size used; hence, fracture toughness, in general, is highest to lowest for the CNB, SEPB and IF methods, respectively [9]. However, this typical trend was not clearly obvious for the MS-70 material, though the CNB method did produce the highest toughness value.

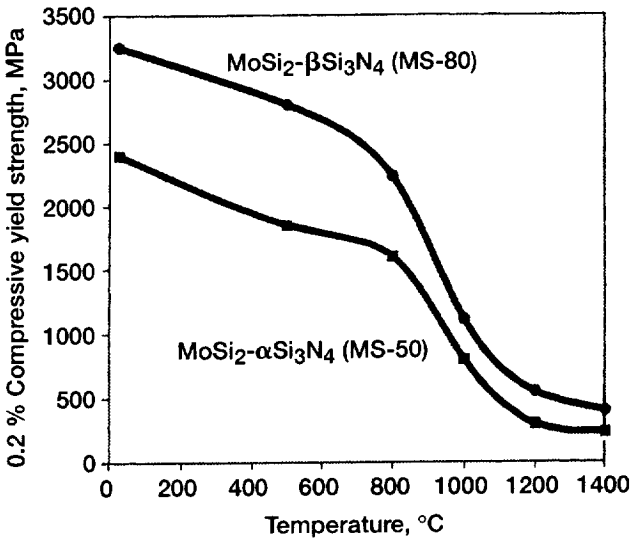

Figure 5.—Compressive yield strength verse temperature for two $MoSi_2$-Si_3N_4 alloys.

Table II.—Fracture Toughness of MS-70 Determined at Room Temperature by Four Different Test Methods

Test method	Conditions	Fracture toughness, K_{IC} (Mpa$\sqrt{m}$)
Indentation Fracture (IF)	5 indents at 98N and 196 N	9.4 ± (0.5)[b]
Single Edge V-Notched Beam (SEVNB)	Three specimens used; $\alpha = 0.25$[a]	7.4 ± (0.4)[b]
Single Edge Precracked Beam (SEPB) (ASTM C1421)	Three specimens used; $\alpha = 0.4$-0.6 [a]	8.9 ± (0.5)[b]
Chevron-Notched Beam (CNB) (ASTM C1421)	Average of five specimens	12.2 ± 0.2

[a]Indicates the ratio of precrack size to specimen depth.
[b]Indicates ±1.0 standard deviation.

It is worth comparing the fracture toughness between $MoSi_2$-βSi_3N_4 (MS-70) and $MoSi_2$-αSi_3N_4 (MS-40 and MS-50). The α-Si_3N_4 reinforced materials exhibited K_{IC} values of 3.5 ± 0.4 MPa$\sqrt{m}$ and 4.9 ± 0.3 MPa$\sqrt{m}$ for MS-40 and MS-50, respectively [10], compared to 8.9 ± 0.5 MPa $\sqrt{m}$ for the in-situ toughened MS-70, as determined by the SEPB method. Therefore, a significant increase in fracture toughness, up to 157 percent by SEPB method, was achieved for MS-70 material through improved material processing and engineered microstructural control. In addition, the fracture toughness of the MS-70 material was greater than that (7.2 ± 0.2 MPa $\sqrt{m}$), of AS-800, an in-situ toughened Si_3N_4 [11]. Figure 6 shows a comparison of the indent crack trajectories generated in the polished surfaces of MS-40, MS-50, and MS-70 materials. Indents were made with a Vickers indenter using an indent load of 98 N. The length of crack emanated from the indent corner was significantly shorter for the MS-70 material, illustrating again that fracture resistance (hence,

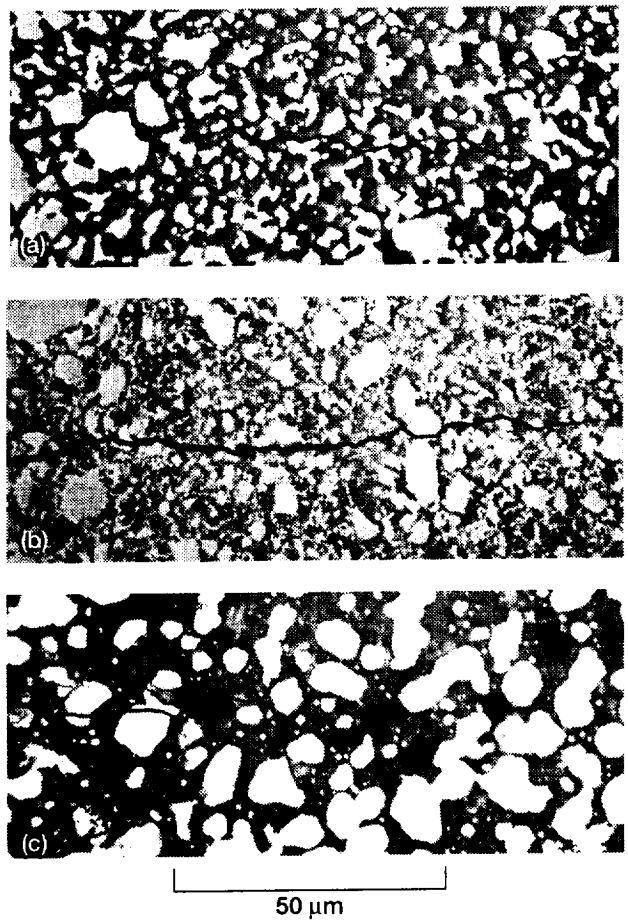

Figure 6.—Indentation crack lengths and trajectories for $MoSi_2$-50 vol percent, Si_3N_4: (a) MS-40, (b) MS-50, and (c) MS-70). An Indent load of 98 N was applied to initiate the cracks.

fracture toughness) was much greater than the MS-40 and MS-50 materials. Also note the more tortuous path of the crack for the MS-70 material.

Room temperature fracture toughness measurements were also made on several chevron notched specimens, machined from the MS-80 $MoSi_2$-βSi_3N_4 material. The microstructure of this material, shown in figure 1(b), indicates the absence of a β-Si_3N_4 whisker morphology. The average K_{Ic} value of this material was only about 5.5 MPa$\sqrt{m}$. This value is very close to the fracture toughness of 4.9 MPa$\sqrt{m}$ for the $MoSi_2$-αSi_3N_4 MS-50) [3,5], which has a similar Si_3N_4 particulate morphology but different phase structure. These results clearly indicate the beneficial effect of the long β-whiskers for improving fracture toughness. In other words, the Si_3N_4 morphology (long whiskers) is responsible for improving the fracture toughness of the material by more than two times compared to blocky Si_3N_4 particulates in $MoSi_2$, regardless of the Si_3N_4 crystal structure.

SEM examination of the fracture surface of $MoSi_2$ *in-situ* whisker-reinforced Si_3N_4 (MS-70), shown in figure 7(a), clearly indicates a tortuous crack path due to the whisker-shaped β-Si_3N_4 and the large $MoSi_2$ particle size. The $MoSi_2$ failed either by cleavage or by cracks

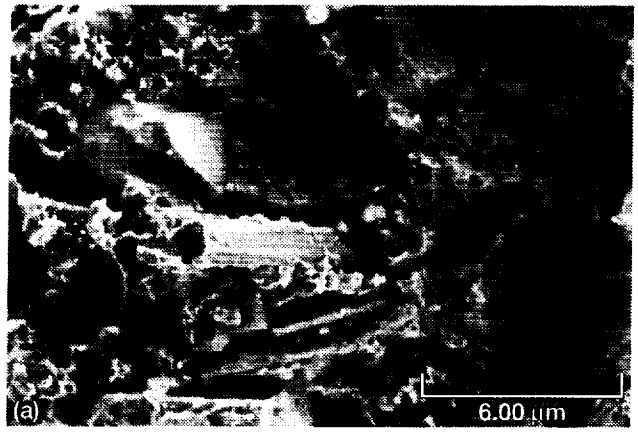

Figure 7.—(a) SEM-secondary electron image of a room temperature fractured surface of $MoSi_2$-βSi_3N_4 (MS-70) samples showing a torturous crack path due to microstructural features such as the long whisker-like morphology of the β-Si_3N_4 and large $MoSi_2$ particle size. (b) SEM-secondary electron image of room temperature fracture toughness tested $MoSi_2$-βSi_3N_4 (MS-80) showing a much planar fracture surface.

circumventing the $MoSi_2$ regions, further increasing the overall crack length. In contrast to figure 7(a), $MoSi_2$-βSi_3N_4 without a whisker morphology exhibits a much more planar fracture path across the material as shown in figure 7(b). The higher fracture toughness of *in-situ* toughened $MoSi_2$-Si_3N_4 (MS-70) compared to $MoSi_2$-Si_3N_4 without the Si_3N_4 whisker morphology or even compared to AS-800 Si_3N_4 is probably derived from combined effects of: (1) efficient crack bridging by the highly elongated Si_3N_4 grains, (2) Si_3N_4 pull-out due to weak bonding with the $MoSi_2$ matrix, and (3) a large particle size for the $MoSi_2$, which combined with weak interfacial bonding promotes crack growth around the $MoSi_2$ phase.

Flexural Strength and Weibull Behavior Figure 8 shows a comparison of the four-point flexural strength of $MoSi_2$-βSi_3N_4 (MS-70), $MoSi_2$-αSi_3N_4 (MS-50) and AS-800 as a function of temperature up to 1400 °C. The data clearly indicate that AS-800 is stronger by about 10 percent than $MoSi_2$-βSi_3N_4 (MS-70) at all temperatures. However, the known potential for further improving the strength by

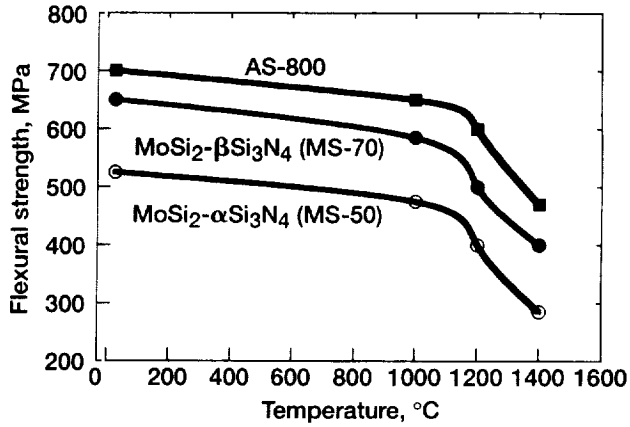

Figure 8.—Flexural strength as a function of temperature for $MoSi_2$-βSi_3N_4 (MS-70) compared to AS-800 and $MoSi_2$-αSi_3N_4 (MS-50).

solid solution and substitutional alloying [12] has not yet been attempted in these particulate composites. Figure 8 also shows that the *in-situ* whisker reinforced $MoSi_2$-βSi_3N_4 (MS-70) is significantly stronger than $MoSi_2$-αSi_3N_4 (MS-50) at all temperatures.

Room-temperature four-point bend tests were carried out to measure the strength and Weibull modulus of two types $MoSi_2$-βSi_3N_4 materials, one with the β-Si_3N_4 in a whisker-like morphology (MS-70) and the other with a more characteristic blocky β-Si_3N_4 particulate structure (MS-80). Weibull parameters were determined from the relationship:

$$\ln \ln (1/1-F) = m_r \ln(\sigma_f/\sigma_r)$$

where σ_f is the fracture strength determined in four-point bending, σ_r is the characteristic strength, m_r is the Weibull modulus and, F is the cumulative failure probability based on

$$F = j\text{-}0.3/J\text{-}0.4$$

where J is the total number of specimens tested and j is the specimen rank assigned by ordering specimens from weakest to strongest. The resulting Weibull distributions for MS-70 and MS-80 are plotted in figure 9. The *in-situ* toughened material (MS-70) exhibits a much higher characteristic strength and Weibull modulus (728 MPa and m=17) than the MS-80 material (461 MPa and m=9.8).

3.4 Environmental Resistance of $MoSi_2$-Si_3N_4 Composites

Low Temperature Oxidation and Pesting Since intermediate-temperature oxidation resistance and pesting phenomena are limiting factors for structural applications of $MoSi_2$-base materials, several critical tests were designed to examine the pesting response. Initially, cyclic oxidation tests were conducted at 400, 500 and 600 °C for 200 cycles. Each cycle consisted of 55 min of heating and 5 min of cooling. The weight gain at 500 °C was comparatively higher than at 400 °C and 600 °C, which confirmed a previous observation [13] that 500 °C is the temperature for maximum accelerated oxidation and pest for $MoSi_2$-base alloys. It was therefore decided that 500 °C would be used for subsequent experiments to examine the intermediate-temperature oxidation behavior in more detail.

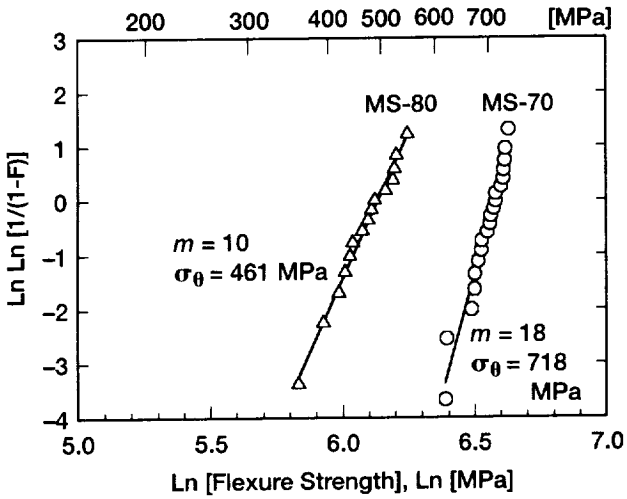

Figure 9.—Weibull (flexure) strength distributions for $MoSi_2$-βSi_3N_4 (MS-70) and (MS-80) materials. *m* and σ_θ represent Weibull modulus and characteristic strength (MPa) of the material, respectively.

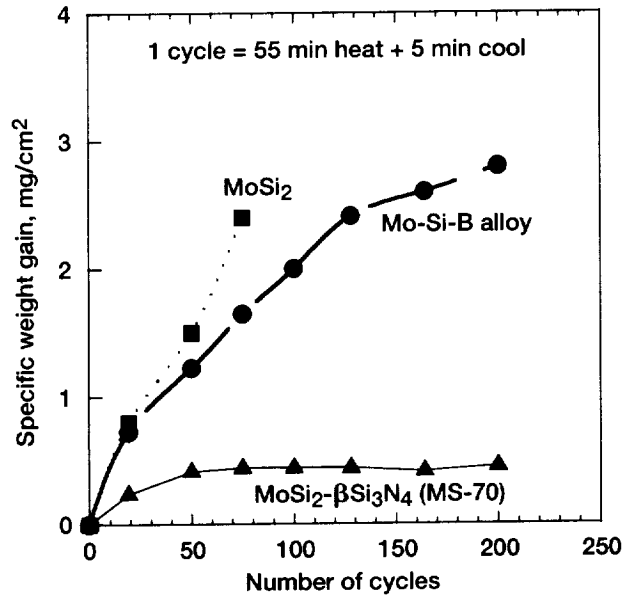

Figure 10.—Specific weight gain versus number of cycles of $MoSi_2$-50βSi_3N_4 (MS-70) at 500 °C compared with $MoSi_2$ and MoSiB alloy.

Figure 10 shows specific weight gain versus number of cycles at 500 °C for $MoSi_2$-βSi_3N_4 (MS-70) and binary $MoSi_2$. The oxidation behavior of a MoSiB alloy (at % 84.5Mo-6.5Si-8B-1Hf) is also included for comparison. There is interest in this alloy, over $MoSi_2$, for structural aerospace applications due to its attractive high-temperature oxidation resistance and good mechanical behavior [14]. However, the $MoSi_2$-βSi_3N_4 (MS-70) shows very little weight gain compared to binary $MoSi_2$ and the MoSiB alloy, indicating the absence of accelerated oxidation. In contrast, the binary $MoSi_2$ and MoSiB alloys exhibited accelerated oxidation followed by pesting. X-ray diffraction analysis of the $MoSi_2$-βSi_3N_4 specimen indicated strong peaks of Si_2ON_2 and the absence of any MoO_3. Previous TEM studies [5,6] of oxidized $MoSi_2$ samples indicated that the oxide formed on $MoSi_2$ has a two-phase lamellar structure consisting of MoO_3 and amorphous SiO_2. This kind of lamellar structure provides an easy diffusion path for oxygen, favoring the formation of the MoO_3 and the start of pesting. TEM examination of a $MoSi_2$-αSi_3N_4 (MS-50) specimen oxidized at 500 °C for 1000 hr showed an order of magnitude decrease in oxide thickness compared to $MoSi_2$ and a disruption of the lamellar oxide structure [3]. However, the Si_2ON_2 phase was not detected in this particular material. Therefore, more work is needed to clearly understand the mechanism of intermediate-temperature oxidation in these materials.

Several other critical oxidation tests were carried out at 500 °C in air to examine the influence of pre-existing cracks and superimposed compressive and tensile stresses on accelerated oxidation and pesting in the *in-situ* toughened $MoSi_2$-βSi_3N_4 (MS-70). In one set of experiments, bend bars were precracked with a Vickers indenter using a 250 N load, and then subjected to 1000 hr at 500 °C, with and without an applied load, with no premature failure or indication of pesting. In another experiment, cylindrical compression specimens were subjected to 500 °C exposure with and without a 20 MPa compressive stress for about 1000 hr. These specimens also exhibited very little oxidation. In another test, a tensile stress of 20 MPa was applied to a button head tensile specimen at 500 °C for about 1000 hr. This specimen also showed no evidence of accelerated oxidation or pesting. Finally, stressed burner-rig tests were conducted on 6-in. long dog-bone shaped tensile specimens, with two different degrees of surface roughness, at 500 °C and 50 MPa tensile stress using a jet fuel burner. Both specimens came away without showing any evidence of pesting or accelerated oxidation. Under similar types of tests, $MoSi_2$ samples would literally be reduced to oxidized powders.

High-Temperature Cyclic Oxidation Cyclic oxidation tests were carried out on rectangular coupons of the in-situ toughened $MoSi_2$-βSi_3N_4 (MS-70) at 1000, and 1350 °C in air for about 100 cycles where each cycle consisted of one hour heating followed by 0.3 hr of cooling. The material exhibited a parabolic oxidation behavior with weight gain of only 0.03 and 0.4 mg/cm^2 at 1000 and 1350 °C, respectively. These weight gain values are smaller than those for AS-800 (0.06 and 0.63 at 1000 and 1350 °C, respectively) [18]. X-ray diffraction of the oxidized surface of the in-situ toughened $MoSi_2$-βSi_3N_4 indicated strong peaks of α-crystobalite, which is a form of SiO_2.

4. Discussion

4.1 Processing of $MoSi_2$-βSi_3N_4

The results from the physical and mechanical testing of several $MoSi_2$-Si_3N_4 materials determined from this investigation clearly indicate that many properties, foremost among them toughness, strength, and mechanical reliability, are very sensitive to microstructure. When the $MoSi_2$-Si_3N_4 alloy is fully dense and the Si_3N_4 is transformed into long whisker-like grains of β-Si_3N_4 (e.g., MS-70 and MS-80) there is an enormous increase in fracture toughness and strength. When the morphology of the Si_3N_4 is something other than whisker-like, these properties are drastically reduced (MS-80). Consequently, it is very important to process these materials properly to exploit the benefits of *in-situ* β-Si_3N_4 whisker reinforcement.

First of all, it is very important to control the chemistry of the powder mixture. The batches of powder processed in the 01-HD attritor (MS-80) appear to be off from the desired composition due to leakage around the seals. This would have particularly affected the very fine Y_2O_3 and Al_2O_3 sintering aids. It is the presence of the sintering aids and the α- to β-Si_3N_4 transformation during consolidation that allows the structure of the Si_3N_4 to evolve into the whisker morphology. It has been found that the a to b transformation occurs in the early stages of liquid phase formation, which is due to melting of the sintering aids. This transformation is not dependent on but rather aids the densification process by forming whisker-like (large aspect ratio) acicular β-Si_3N_4 grains from of the parent α-Si_3N_4 particles. Both the transformed β-Si_3N_4 grains and those present in the initial powder then tend to grow via coalescence through a dissolution-precipitation reaction.

Second, it is desirable to achieve full densification during hot pressing, otherwise it is necessary to can the material prior to HIP'ing. HIP processing at very high temperatures is necessary in order for the Si_3N_4 to grow into the β-Si_3N_4 whisker-like structures as discussed above. Hot pressing at conditions as high as 1700 °C and 56 MPa pressure is not sufficient to achieve full densification of this material. While hot pressing at 1800 °C and 70 MPa pressure is sufficient to fully densify $MoSi_2$-Si_3N_4, these conditions exceed the capability of most hot-press tooling, including all graphite materials. However, HIP'ing without a can also has its drawbacks. It is important to use high quality Ar gas during HIP'ing to prevent oxidation of the compact or it is necessary to use a gettering scheme that does not react with the $MoSi_2$-Si_3N_4. For example, graphoil is not stable at high temperatures beyond 1700 °C and diffuses into $MoSi_2$ and Si_3N_4 mixtures to form SiC and nitrogen gas that inhibits the β-Si_3N_4 grain growth.

Furthermore, a two-step process of hot pressing and HIP'ing is very expensive and hence not attractive for industrial manufacturing of $MoSi_2$ –*in-situ* toughened β-Si_3N_4. If hot pressing could be done in one step using high temperatures and pressures to achieve full density along with β-Si_3N_4 grain growth, then it may become more attractive for industrial production. Unfortunately, high performance graphite dies (e.g., made from ISO-60 graphite) cannot handle the temperatures and pressures needed. Hot pressing dies made from W-Re alloys or C-C composites can probably handle these temperatures and pressures, but unfortunately these materials react very severely with $MoSi_2$ powder. Another alternative is to use a one step HIP operation using either refractory metals such as Nb or Ta, or glass as canning materials. It may be possible to achieve full consolidation and grain growth in one step, making this a more attractive processing route. Work is in progress to investigate this possibility.

Even so, hot pressing and HIP'ing does not lead to near net shape component fabrication. Advanced powder metallurgy processing techniques such as laser-beam assisted rapid proto typing and low pressure plasma spraying may be used to cost effectively manufacture complex aerospace structures made from $MoSi_2$-βSi_3N_4 powders. Work is also in progress to evaluate these two techniques for production of $MoSi_2$-βSi_3N_4 components with initial success demonstrated in recent low-pressure plasma spray trials.

4.2 Reasons for the Enhanced Toughness of in-situ Whisker Reinforced $MoSi_2$-βSi_3N_4

The toughening mechanisms operative in the *in-situ* whisker reinforced $MoSi_2$-βSi_3N_4 are crack deflection, crack bridging, and grain pull-out. Faber and Evans [19] considered the problem of a dispersed second phase consisting of cylindrically shaped particles that deflect the crack along its long axis. In such materials the crack front would twist in and out along the long axis and so they concluded that the twist component of the deflected crack increases the fracture toughness.

Crack bridging, on the other hand, connects the two faces of a crack with a load-bearing element behind the crack tip. These ligaments carry some of the stress and reduce the stress intensity at the crack tip. In β-Si_3N_4, the long grains remain attached to both faces of the crack and become the load bearing ligaments. After the bridging grains break or detach from the crack face, other mechanisms, such as pull-out become active. The stress necessary to overcome the frictional stress of pull-out also reduces the stress intensity at the crack tip. These mechanisms operate behind the wake of the crack front leading to R-curve behavior by increasing the stress necessary to propagate a crack by applying a closure stress on the crack wake [20]. The closure stress on the crack wake is a function of the crack length because the number of bridging grains and pulled out grains in the crack wake increases as the crack grows. Thus, crack bridging and grain pull-out are dominant toughening mechanisms in materials with dispersed elongated reinforcements [21].

Through a combination of these three toughening mechanisms (crack deflection, bridging, and pull-out), the *in-situ* whisker reinforced $MoSi_2$-βSi_3N_4 exhibited significant toughness compared to materials of similar composition. In both the $MoSi_2$-αSi_3N_4 (MS-50 and MS-40) and the MS-80 material, the Si_3N_4 did not possess a whisker structure and hence these material only underwent crack deflection resulting in a lower fracture toughness. Furthermore, because the additional toughening mechanisms, such as bridging and pullout, lead to a rising R-curve behavior, the *in-situ* whisker reinforced $MoSi_2$-βSi_3N_4 would be expected to have better reliability (that is higher Weibull modulus and characteristic strength for the same population of flaws). Because the results do indicate a higher Weibull modulus and strength for MS-70 compared to other $MoSi_2$-base materials, then either the flaw population in this material is unusually uniform or a rising R-curve behavior is active during fracture. Another consequence of R-curve behavior would be discrepancies in fracture toughness values obtained from the different testing techniques as summarized in table II.

5. Summary and Conclusions

A new $MoSi_2$-based composite with an engineered microstructure consisting of large particles of $MoSi_2$ reinforced with long whisker-shaped grains of Si_3N_4 was developed by careful control of alloy chemistry and consolidation techniques. This in-situ toughened $MoSi_2$-βSi_3N_4 exhibited higher fracture toughness and Weibull modulus than other $MoSi_2$–base materials or a structural Si_3N_4 ceramic. This higher fracture toughness and structural reliability is derived from crack bridging and grain pull out of the highly

elongated Si_3N_4. This material also exhibits excellent resistance to intermediate-temperature pesting that affects most other Mo-base and $MoSi_2$-base alloys. Given this combination of good fracture resistance and excellent environmental resistance, which is superior to most other Mo-base alloys, the in-situ toughened $MoSi_2$-βSi_3N_4 developed in this study shows great promise as a high-temperature structural material. However, the development of reliable, cost-effective processing methods will be needed to broaden interest in this material.

References

1. A.K. Vasudevan and J.J. Petrovic, in High Temperature Silicides, ed. A.K. Vasudevan and J.J. Petrovic, North Holland, NY, 1992, pp. 1–17.

2. M.G. Hebsur, in Intermetallic Composites III, ed. J.A. Graves, R.R. Bowman, and J. Lewandowski, MRS Proc. vol. 350, Pittsburgh, PA, 1994, pp. 177–182.

3. M.G. Hebsur and M.V. Nathal, in Structural Intermetallics 1997, ed. M.V. Nathal, et al., TMS, Warrendale, PA, 1997, pp. 949–958.

4. M.G. Hebsur, "Pest resistant $MoSi_2$ materials and method of making," U.S. Patent, No. 5,429,997 (1995).

5. M.G. Hebsur, *Mater. Sci. & Eng.*, A261, (1999), pp. 24–37.

6. M.G. Hebsur, in Materials Aging and Life Management, ISOMALM, ed. Braj, et al., 2000, pp. 749–757.

7. K. Yamada and N. Kamiya, *Mat. Sci. & Eng.*, A261, (1999), pp. 270–277.

8. J. Kübler, "Fracture Toughness of Ceramics using the SEVNB Method: Round Robin," VAMAS Report No. 37, Swiss Federal Laboratories for Materials Testing & Research (EMPA), Dübendorf, Switzerland (1999).

9. S.R. Choi and J.A. Salem, *J. Am. Ceram. Soc.*, 77, (1994), pp. 1042–1046.

10. S.R. Choi, and M.G. Hebsur, *Ceram. Eng. Sci. Proc.*, 19, (1999), pp. 361–369.

11. S.R. Choi and J.P. Gyekenyesi, *Trans. of the ASME, J. Eng. for Gas Turbines & Power*, 121, (1999), pp. 18–24.

12. D.M. Shah and D.L. Anton, U.S. Air Force Report WRDC–TR–90–4122, Feb. 1991.

13. S. Bose, in High Temperature Silicides, ed. A.K. Vasudevan and J.J. Petrovic, North-Holland, NY, 1992, pp. 217–225.

14. D.M. Berczik, "Oxidation Resistant Molybdenum Alloy," U.S. Patent, No. 5,696,150 (1997).

15. E. Fitzer and W. Remmele, in 5th Int. Conf. on Composite Materials, ICCM-V, TMS-AIME, Warrendale, PA, 1985, pp. 515–530.

16. W.D. Forgeng and B.F. Decker, *Trans. AIME*, 212, (1958), pp. 343–348.

17. V.K. Sarin, *Mat. Sci. and Eng.*, A105/106, (1988), pp. 151–159

18. Chien-Wei Li, AlliedSignal Report, August 1993.

19. K.T. Faber and A.G. Evans, *Acta Metall.*, 31, (1983), pp. 577–584.

20. V. Tikare, S.R. Choi and J.A. Salem, in In-Situ Composites, Science and Technology, ed. by. M. Singh and D. Lewis, TMS, Warrendale, PA, 1994, pp. 193–210.

21. J. Rodel, *J. European Ceram. Soc.*, 10, (1992), pp. 143–150.

REPORT DOCUMENTATION PAGE

Form Approved
OMB No. 0704-0188

1. AGENCY USE ONLY (*Leave blank*)	2. REPORT DATE	3. REPORT TYPE AND DATES COVERED
	May 2001	Technical Memorandum

4. TITLE AND SUBTITLE

Development of Tough, Strong, and Pest-Resistant $MoSi_2$-βSi_3N_4 Composites for High-Temperature Structural Applications

5. FUNDING NUMBERS

WU-708-31-13-00

6. AUTHOR(S)

M.G. Hebsur, S.R. Choi, J.D. Whittenberger, J.A. Salem, and R.D. Noebe

7. PERFORMING ORGANIZATION NAME(S) AND ADDRESS(ES)

National Aeronautics and Space Administration
John H. Glenn Research Center at Lewis Field
Cleveland, Ohio 44135-3191

8. PERFORMING ORGANIZATION REPORT NUMBER

E-12714

9. SPONSORING/MONITORING AGENCY NAME(S) AND ADDRESS(ES)

National Aeronautics and Space Administration
Washington, DC 20546-0001

10. SPONSORING/MONITORING AGENCY REPORT NUMBER

NASA TM—2001-210807

11. SUPPLEMENTARY NOTES

Prepared for the International Symposium on Structural Intermetallics cosponsored by The Minerals, Metals, and Materials Society and the American Institute of Mining, Metallurgical, and Petroleum Engineers, Jackson Hole, Wyoming, September 23–25, 2001. M.G. Hebsur and S.R. Choi, Ohio Aerospace Institute, 22800 Cedar Point Road, Brook Park, Ohio, 44142; J.D. Whittenberger, J.A. Salem, and R.D. Noebe, NASA Glenn Research Center. Responsible person, M.G. Hebsur, organization code 5120, 216–433–3266.

12a. DISTRIBUTION/AVAILABILITY STATEMENT

Unclassified - Unlimited
Subject Category: 29 Distribution: Nonstandard

Available electronically at http://gltrs.grc.nasa.gov/GLTRS

This publication is available from the NASA Center for AeroSpace Information, 301–621–0390.

12b. DISTRIBUTION CODE

13. ABSTRACT ***(Maximum 200 words)***

A new $MoSi_2$-base composite was developed that contains *in-situ* reinforcement of whisker-type β-Si_3N_4 grains in a $MoSi_2$ matrix. The advantages of this *in-situ* reinforced $MoSi_2$-Si_3N_4 are lower density, higher fracture toughness and better strength than typical $MoSi_2$ alloys, combined with excellent environmental and pest resistance. The average fracture toughness of the *in-situ* reinforced material determined by one technique was 12.2 MPa$\sqrt{m}$ compared to 4.9 to 5.5 MPa$\sqrt{m}$ for similar materials with the exception that the β-Si_3N_4 had a blocky morphology as opposed to the whisker-like morphology typical of the *in-situ* toughened material. This $MoSi_2$-βSi_3N_4 was also resistant to pesting at intermediate temperatures (400 to 600 °C) even when precracked or under applied load; conditions that would quickly reduce typical $MoSi_2$ alloys to oxidized powder.

14. SUBJECT TERMS

$MoSi_2$ intermetallic; *in-situ* toughening; pesting; fracture toughness; Weibull modulus; β-Si_3N_4 whiskers

15. NUMBER OF PAGES

16

16. PRICE CODE

17. SECURITY CLASSIFICATION OF REPORT	18. SECURITY CLASSIFICATION OF THIS PAGE	19. SECURITY CLASSIFICATION OF ABSTRACT	20. LIMITATION OF ABSTRACT
Unclassified	Unclassified	Unclassified	